https://doi.org/10.5194/egusphere-2022-814
Preprint. Discussion started: 23 August 2022

Drivers of Particle Sinking Velocities in the Peruvian Upwelling System

Moritz Baumann[1], Allanah Joy Paul[1], Jan Taucher[1], Lennart Thomas Bach[2], Silvan Goldenberg[1], Paul Stange[1], Fabrizio Minutolo[3], Ulf Riebesell[1]

[1]Biological Oceanography, GEOMAR Helmholtz Centre for Ocean Research Kiel, Kiel, Germany
[2]Institute for Marine and Antarctic Studies, University of Tasmania, Hobart, Tasmania, Australia
[3]Helmholtz Centre Hereon, Institute of Carbon Cycles, Geesthacht, Germany

Correspondence to: Moritz Baumann (mbaumann@geomar.de)

Abstract. As one of Earth's most productive marine ecosystems, the Peruvian Upwelling System transports large amounts of biogenic matter from the surface to the deep ocean. Whilst particle sinking velocity is a key factor controlling the biological pump, thereby affecting carbon sequestration and O_2-depletion, it has not yet been measured in this system. During a 50-day mesocosm experiment in the surface waters off the coast of Peru, we measured particle sinking velocities and their biogeochemical and physical drivers. We further characterized the general properties of exported particles under different phytoplankton communities and nutritional states. Average sinking velocities varied between size classes and ranged from 12.8 ± 0.7 m d^{-1} (particles 40–100 µm), to 19.4 ± 0.7 m d^{-1} (particles 100–250 µm), and 34.2 ± 1.5 m d^{-1} (particles 250–1000 µm) (± 95% CI). Surprisingly, no relationship between opal ballast and sinking velocity could be identified, despite the presence of diatoms, questioning the importance of opal ballast in freshly produced material sinking from the surface. In contrast, we found higher sinking velocities with increasing particle size, compactness and roundness. Size had by far the strongest influence among these physical particle properties. Our study provides a detailed analysis of the drivers of particle sinking velocity in the Peruvian Upwelling System, which allows modelers to optimize local particle flux parameterization. This will help to better project oxygen concentrations and carbon sequestration in a region that is subject to substantial climate-driven changes.

1 Introduction

The Peruvian Upwelling System is one of the most productive marine ecosystems in the world (Pennington et al., 2006). It is situated along the Peruvian and northern Chilean coasts in the boundary current system of the Eastern Tropical South Pacific and is one of four major Eastern Boundary Upwelling Systems (EBUS). It is characterized by strong Ekman-transport-induced upwelling of nutrient-rich subsurface water along the coast, which results in a shallow thermocline that confines an optimal phytoplankton habitat. The high primary productivity of Peru's "brown waters" sustains a rich ecosystem with abundant fish and other larger organisms and leads to the vertical transport of large amounts of biogenic matter (Kämpf and Chapman, 2016). This sinking flux fuels high respiration rates in the subsurface, which in combination with slow ventilation

https://doi.org/10.5194/egusphere-2022-814
Preprint. Discussion started: 23 August 2022

results in permanently oxygen deficient waters (Chavez and Messié, 2009). These can start at 50 m depth and shallower (Kämpf and Chapman, 2016; Karthäuser et al., 2021a), stretch hundreds of meters of depth (Karstensen et al., 2008) and extend up to 1000 km from the coast. The dimensions and biogeochemical properties of this oxygen minimum zone (OMZ) are directly affected by the amount and properties of sinking material (Kalvelage et al., 2013; Karthäuser et al., 2021b).

A key metric of sinking biogenic matter is the velocity with which particles settle (e.g. Marsay et al., 2015). Sinking velocity influences the transfer efficiency of biogenic matter to depth and hence the export of carbon via the biological pump, which sequesters CO_2 in the ocean interior (Khatiwala et al., 2013; McDonnell et al., 2015). In the Peruvian Upwelling System, sinking velocity additionally determines the length of exposure of a particle to deoxygenated OMZ waters. Here, the degradation of small sinking particles (<500 µm) might contribute significantly to the loss of nitrogen via anammox (Karthäuser et al., 2021b) and hence to the sustained presence of the subsurface OMZ.

Sinking velocity is controlled by a variety of physical characteristics. A particle's excess density compared to sea water ultimately determines whether it sinks and how fast. Amongst particles of the same composition and structure, larger particles sink faster (Riley et al., 2012). Yet, a small but dense particle can also sink fast (McDonnell and Buesseler, 2010). Although a size-sinking velocity relationship has not been detected in some observational datasets (Iversen and Lampitt 2020), a recent meta-analysis resolved a relatively weak but clear relationship (Cael et al., 2021). Particle size is hence considered relevant, but not the primary factor determining sinking velocity.

Particle density and size are dependent on biological processes, which influence the structure, shape and composition of a particle. Diatom blooms can produce large cells with appendages, that promote aggregation, and can lead to fast sinking matter (Smetacek et al., 2012). An oligotrophic phytoplankton community, on the other hand, consists of smaller cells, which tend to sink slower (Guidi et al., 2009). Biomineral ballast produced by phyto- and zooplankton is denser than organic matter (calcium carbonate, opal and organic matter densities: 2.71, 2.1 and ~1.06 g cm^{-3}, respectively; Klaas and Archer 2002) and can enhance particle sinking velocities (Armstrong et al., 2009). Furthermore, the porosity of a particle (i.e. the fraction of particle volume occupied by seawater) affects its density (Laurenceau-Cornec et al., 2020). If organic matter is densely packed, e.g. by zooplankton into a fecal pellet, it has a higher excess density and sinks faster compared to one that is packed more loosely (Steinberg and Landry, 2017; Bach et al., 2019). The plankton community structure thus influences physical characteristics of sinking particles (Bach et al., 2019; Turner, 2015; Guidi et al., 2009).

Here, we report sinking velocities and physical particle properties of more than 100.000 individual particles collected during a mesocosm study in the Peruvian Upwelling System (Bach et al., 2020). We determine relationships between velocity and particle size, shape and porosity. We further assessed how sinking velocities change with the quantity and stoichiometry of the overall export flux, as well as with the proportion of biogenic ballast, and try to decipher the influence of the prevailing phytoplankton community. Our study provides insights into the controls of particle sinking velocity, a key aspect of carbon sequestration and OMZ shaping processes.

https://doi.org/10.5194/egusphere-2022-814
Preprint. Discussion started: 23 August 2022

2 Materials and Methods

2.1 Experimental Setup

Our experimental setup consisted of eight sea-going mesocosms (M1–M8, see Riebesell et al., 2013), which were moored in the coastal upwelling area off Callao, Peru (12.06°S, 77.23°W), on February 23rd, 2017 (late austral summer). The top and bottom openings were equipped with screens of 3 mm mesh size to keep larger organisms such as small pelagic fish out of the mesocosms. The mesocosms were left fully submerged for two days after mooring to ensure a flow-through of surrounding Pacific water. Afterwards, the two screens of each mesocosm were removed, the top was pulled above sea level and a cone-shaped sediment trap was attached to the bottom, thereby enclosing a pelagic community inside the mesocosms. They contained ~54 m^3 of sea water and extended 19 m below the water surface. The closing of the mesocosms marked the start of the experiment (t0, February 25th), which lasted for 50 days until April 16th.

To simulate an upwelling event and test the effect of oxygen minimum zone (OMZ)-influenced water masses on the natural plankton community, we collected two different OMZ-influenced water batches and added them to the mesocosms. The batches differed from each other in terms of NO_x^- (nitrate + nitrite) concentrations. One had low and the other very low NO_x^- concentrations of 4 and 0.3 µmol L^{-1}, respectively, compared to the naturally occurring waters of the coastal upwelling area. Our OMZ treatment thus had two levels: low NO_x^- and very low NO_x^-. The upwelling event was simulated on t11 and t12 by replacing 20 m^3 of mesocosm water with OMZ-influenced water in every mesocosm. Mesocosms M1, M4, M5 and M8 received water from station 1 (low NO_x^-), whereas mesocosms M2, M3, M6 and M7 were fertilized with water from station 3 (very low NO_x^-). Figure 2 in Bach et al. (2020) shows the changes in the dissolved nutrient pools following the additions.

An overview of the basic system parameters, as well as detailed information on the experimental setup, mesocosm maintenance, sampling procedure and sample analysis is given in the overview paper by Bach et al. (2020).

2.2 Sampling procedure

Long silicon tubes were connected to the bottom of the sediment traps, through which sedimented matter was sampled using a manual vacuum pump (< 0.3 bar, see Boxhammer et al., 2016). The sediments were pumped into 5L glass bottles (Schott, Denmark), which were stored dark and cool until arrival in the lab. There, the sample bottles were gently rotated and the mixed sediment suspension was subsampled for particle sinking velocity measurements using a pipette.

Bulk water column samples were taken at least every second day and were used for a variety of parameters, among which were chlorophyll *a* and phytoplankton community composition (Bach et al., 2020). Depth-integrated water samples were taken using 5 L water samplers equipped with pressure sensors (Hydro-Bios, Germany). The samples were transferred into 10 L carboys and transported to the on-shore laboratories.

https://doi.org/10.5194/egusphere-2022-814
Preprint. Discussion started: 23 August 2022

2.3 Sample analysis

All samples were processed in on-shore laboratories inside the Club Náutico Del Centro Naval and the Instituto del Mar del Perú (IMARPE), both located in La Punta (Callao), and were either measured directly or prepared for transport to the GEOMAR Helmholtz-Centre for Ocean Research Kiel for later analyses.

2.3.1 Sinking velocity and particle properties

Sinking velocity and optical particle properties were measured via video microscopy using the method described in Bach et al. (2012) and further developed in previous studies (Bach et al., 2019; Baumann et al., 2021). The sediment subsamples were transferred to a sinking chamber (edge length: 1 x 1 cm), which was mounted vertically in a FlowCam device (Fluid Imaging Technologies, United States). The trajectories of sinking particles were recorded for 20 min at ~7 frames per second and sinking velocities were calculated by fitting a linear model to the vertical positions and time stamps of multiple captures of the same particle. Besides position and time, the FlowCam measured proxies for several physical particle properties for each individual particle. Particle size was estimated as equivalent spherical diameter (ESD), shape as the aspect ratio (length to width ratio) and porosity as a size-normalized measure for particle intensity (P_{int}). To calculate the porosity-proxy, each particle image was transformed to a greyscale with dark pixels considered optically opaque (low intensity) and bright pixels translucent (high intensity, pixel intensity ranging from 0 to 255). The underlying assumption is that a particle looks brighter when it is more porous, compared to a darker-appearing particle. Since larger particles are generally more porous than smaller ones (Laurenceau-Cornec et al., 2020), we combined the intensity value with particle size (i.e. ESD) and calculated porosity (P_{int}) following Bach et al. (2019).

$$P_{int} = (intensity/255)^2 * ESD \quad (1)$$

Particles out of focus were excluded from the analysis based on their sharpness. Sinking velocities were corrected for wall effects of the sinking chamber using the equation given in Ristow (1997). Measurements were carried out in a temperature controlled lab, which was set to daily *in situ* temperatures of between 16 and 21 °C. Calculations were done using the MATLAB script described by Bach et al. (2012), which was adjusted for a broader particle size spectrum (40–1000 µm). Further data analysis was carried out using the R software (R Core Team, 2021; version 4.1.2), and the package "tidyverse" (Wickham et al., 2019).

The size distribution of the measured particles was heavily right-skewed, i.e. there were far more small than large particles. Based on the ESD, the sinking velocity data were thus separated into three size classes, 40–100 µm, 100–250 µm, and 250–1000 µm. The increasing bin widths thereby consider the particle size distribution, resulting in narrower size classes for small particles and broader ones for larger particles. Due to the relatively low contribution of large particles in general, for some measurements there were too few particles in the large size class to be considered for further analysis. We hence removed the 250–1000 µm size class of those measurements that consisted of fewer than 3 particles. This affected the

https://doi.org/10.5194/egusphere-2022-814
Preprint. Discussion started: 23 August 2022

measurements of M5 and M7 on T32, as well as M5 on T40, and M7 on T48. The right-skewed size distribution was also the reason why we plotted the median ESD, porosity and aspect ratio in Fig. 3a, since the mean would have given the few large particles undue weight.

Furthermore, our sinking velocity and ESD measurements of all particles measured across mesocosms were collated and used to resolve the relationship between sinking velocity and particle size, following the power function of Cael et al (2021, Eq. 3).

$$SV(ESD) = \alpha * ESD^{\beta} \quad (2)$$

Here, α and β are scaling factors, whose variability is based on the particle characteristics and environmental conditions (e.g. composition, porosity, temperature). They were estimated for our data set using the linearized logarithmic function.

$$\log SV = \beta * \log ESD + \log \alpha \quad (3)$$

In order to not give the numerous small particles in our measurements undue weight, the sinking velocity and ESD data were binned into log-spaced size classes (40–63, 63–100, 100–158, 158–251, 251–398, 398–631, 631–1000). Per size class, log(sinking velocity) and log(ESD) means from all eight mesocosms were calculated for each experimental day. Based on these, size-sinking relationships were calculated by fitting linear models, in which the slope represented the scaling factor β and the y-intercept log(α). From these daily α and β coefficients average values (± SD) over time were calculated, and the corresponding relationships were plotted in Fig. 4 (Sect. 4.2.3). Since the largest size class (631–1000 µm) had too few particle counts (<500 particles), in order to calculate a meaningful and representative size-sinking relationship, we only used the size classes between 40 and ~630 µm.

2.3.2 Elemental analysis of sediment trap samples

The remaining sediment trap samples were prepared for elemental analysis by removing the particulate material from the water. For this, the samples were treated with 3 M $FeCl_3$ to induce particle flocculation, coagulation and subsequent sedimentation inside the 5 L bottle and with 3 M NaOH to adjust the pH to 8.1. Subsequently, they went through multiple centrifugation steps (see Bach et al., 2020 for details), after each of which the supernatant was carefully decanted. The resulting sediment pellets were deep-frozen and transported to Kiel, where they were freeze-dried to remove the remaining moisture. The dry pellets were ground in a ball mill, which produced a fine homogeneous powder (Boxhammer et al., 2016). Representative subsamples of the sediment powder were analyzed for their contents of particulate organic carbon and nitrogen (POC/PON), particulate inorganic carbon (PIC, i.e. calcium carbonate), biogenic silica (BSi, i.e. opal) and total particulate phosphorus (TPP). In contrast to the sinking velocity measurements, the elemental analysis of sediment samples was not carried out for single particles, but for the bulk particulate matter flux.

TPP and BSi contents were measured spectrophotometrically after Hansen and Koroleff (1999) and C and N contents were measured on an elemental analyzer (EuroEA) following Sharp (1974). While PON samples were measured directly,

https://doi.org/10.5194/egusphere-2022-814
Preprint. Discussion started: 23 August 2022

subsamples for POC were fumed with 1 mol L^{-1} HCl and dried at 50 °C overnight to remove the inorganic carbon fraction prior to its measurement. PIC was calculated as the difference between the carbon contents of HCl-untreated and HCl-treated subsamples, i.e. between subsamples containing inorganic carbon and subsamples not containing any. Total mass fluxes to the sediment trap were obtained by upscaling the measured contents of each compound to the total sample weight. Mass fluxes were then normalized to the mesocosm volume and the time between sampling collection (48 h) to obtain mass flux data in µmol L^{-1} d^{-1}.

We further calculated the relative contribution of opal and calcium carbonate to the total export flux, i.e. their biomineral weight fractions (BSi_{WF} and PIC_{WF}), on each sampling day according to Bach et al. (2016) as

$$biomineral_{WF} = \frac{biomineral_{ST} * density_{biomineral}}{1.06 * POC_{ST} + 2.1 * BSi_{ST} + 2.7 * PIC_{ST}} \quad (4)$$

where 'biomineral' stands for either BSi or PIC, and POC_{ST}, BSi_{ST} and PIC_{ST} are the daily mass fluxes to the sediment trap of the respective compound.

2.3.3 Chlorophyll *a* and phytoplankton pigments

Samples for chlorophyll *a* and other phytoplankton pigments were filtered through combusted (450 °C, 6h) GF/F glass fiber filters (0.7 µm pore size, Whatman) in the on-shore laboratories. Directly after filtration the filters were flash-frozen in cryo-vials and stored at -80 °C. Back in Kiel, phytoplankton pigments were extracted from the filters using 100 % acetone as described by Paul et al. (2015) and then analyzed using reverse-phase high-performance liquid chromatography (HPLC, Barlow et al., 1997). The output was analyzed using CHEMTAX, which classifies phytoplankton taxa based on their pigment ratios (Mackey et al., 1996) and allows to estimate the contribution of different phytoplankton taxa to the total amount of chlorophyll *a*. We employed the reference pigment ratios described for the Peruvian Upwelling System by DiTullio et al. (2005).

2.3 Data analysis

Linear mixed effects models were used to investigate the relationship between our predictors and particle sinking velocity as central response variable. *Day* (of the experiment) was always employed as categorical fixed effect and *Mesocosm* as random effect (n=8, random intercept) to account for the repeated measures of the mesocosms over time. The models were fitted using restricted maximum likelihood. Analysis of variance was used to test for significances of the fixed effects (type III test, Satterthwaite's approximation, $\alpha = 0.05$).

Firstly, we tested the effect of the upwelling with different oxygen minimum zone water (*OMZ*, categorical with 2 levels: very low and low NO_x). Average *sinking velocity* of each size fraction (40–100, 100–250 and 250–1000 µm) was modelled as a function of *OMZ*, *Day* and their interaction (*OMZ* × *Day*). We only included data obtained after the application of the treatment (OMZ water addition on t11/t12). *OMZ* × *Day* or *OMZ* was clearly insignificant for all size classes (all p-values

https://doi.org/10.5194/egusphere-2022-814
Preprint. Discussion started: 23 August 2022

>0.318, see Table A1 in the Appendices). For the purpose of parsimony, we therefore removed the factor *OMZ* from all our subsequent investigations. The appropriateness of this exclusion was verified by fitting all following models once with and once without *OMZ*, finding it to be highly insignificant in every instance.

Secondly, we explored the influence of biogeochemical properties of the export flux (continuous predictors), that are, in turn, a result of the current state of the pelagic system. The average *sinking velocity* of each size fraction (40–100, 100–250 and 250–1000 µm) was modelled as a function of *Day* and a series of continuous fixed effects including the magnitude of the export flux (POC_{ST}), its elemental composition (N_{ST}:P_{ST}) and the contribution of biominerals (BSi_{WF} and PIC_{WF}).

Thirdly, we modelled the relationship between sinking velocity and physical particle properties. *Sinking velocity* was modelled as a function of *Day* and the continuous fixed effects particle size (*ESD*), particle porosity (P_{int}) and shape (*Aspect ratio*, i.e. length to width ratio). Here, we could use individual particles as the lowest level of replication, as the FlowCam data provided matching measures of physical properties and sinking velocity for hundreds of particles per mesocosm and day, resulting in an N > 100,000 particles. In order to account for the relatedness of particles measured within the same sample, the factor *Sample* was added as additional random effect (random intercept) nested within *Mesocosm*. Since porosity is dependent on size in Eq. 1, we assured that there was no autocorrelation between size and porosity (in a tentative model fit without interaction terms).

Statistical analysis was carried out using R (R Core Team, 2021). The packages lme4 (Bates et al., 2015) and lmerTest (Kuznetsova et al., 2017), sjstats (Lüdecke, n.d.) and performance (Lüdecke et al., 2021) were used to fit and test linear mixed effect models, calculate partial effect sizes (partial eta squared = η_p^2) and check assumptions, respectively. The normality of residuals and random effects were checked using Q-Q plots and the homogeneity of variance using residuals versus fitted plots. Data was transformed where necessary. Autocorrelation was tested for using Durbin-Watson tests. Multicollinearity was assessed by calculating the variance inflation factor and assessing the correlations between predictors. The fitted models were checked for influential data points using Cook's distance and detected outliers removed.

3 Results

3.1 Particle sinking velocities and phytoplankton community succession

We observed average sinking velocities of 12.8 ± 0.7 m d^{-1} (particle size: 40–100 µm), 19.4 ± 0.7 m d^{-1} (particle size: 100–250 µm), and 34.2 ± 1.5 m d^{-1} (particle size: 250–1000 µm) (± 95% CI, Fig. 1a–c). Sinking velocities increased almost threefold from the smallest to the largest size class. The variability in sinking velocities of bulk sediment samples across space and time is indicated by standard deviations of 0.8, 0.9, and 1.8 m d^{-1} from the smallest to the largest size fraction, respectively. Individual particles were much more variable, however, ranging from <1 to 267 m d^{-1}.

https://doi.org/10.5194/egusphere-2022-814
Preprint. Discussion started: 23 August 2022

The oxygen minimum zone (OMZ) treatment did not affect sinking velocities in any of the particle size classes over the course of the experiment (Fig. 1 and Table A1). Any potential signal of the OMZ treatment (red and blue lines) must have been minor compared to the variability caused by other processes, so that mesocosms appeared to be distributed randomly around the overall mean (Fig. 1).

In contrast, pronounced temporal trends in sinking velocity were detected in all size classes, represented by the factor Day (Fig. 1 and Table A1). Depending on the size class, between 42 % and 48 % of the variation in sinking velocity was explained by our models (see R^2 in Table A1), primarily via this temporal effect. Generally, sinking velocities started high, progressively fell and reached their minimum in the middle of the experiment before rising again to higher levels towards the end.

We observed a distinct phytoplankton community succession, which is linked to both suspended and exported particulate matter and ultimately particle sinking velocities. Following these major biogeochemical developments, we segmented the experiment into three distinct phases: phase I (t1–t20), phase II (t20–t40) and phase III (t40–t50) (for details see Bach et al. (2020). The conditions inside the mesocosms were initially N-replete and sustained diatom-dominated communities (Fig. 1e). Although the OMZ water addition on t11/t12 enriched the dissolved inorganic nutrient pools slightly, these nutrients were readily taken up, and the systems became N-deplete at around t20 (see Fig. 4 in Bach et al. 2020). The decline in diatom dominance as nutrients became depleted coincided with a gradual decrease in sinking velocities of exported particles. The sinking of the smaller, yet most abundant particles slowed down in particular, with more than 50 % lower sinking velocities on t20 compared to the beginning when diatoms dominated. The community shifted towards the mixotrophic dinoflagellate *Akashiwo sanguinea*, which thrived under the regenerative conditions, and sinking velocities reached their minimum between t20 and t30. Finally, during the last ten days of the experiment (t40–t50) seabirds (Inca tern, *Larosterna inca*) started to use the mesocosm facilities as a resting place, defecating into the mesocosms and thereby providing new N and P, fueling new production (Fig. 1d). Simultaneously, sinking velocities reached another maximum towards t50, this time especially in the medium and large size classes.

3.2 Export flux and biomineral ballast

We could not detect an influence of particle sinking velocities on the magnitude and quality of the export flux in any of the size classes (Fig. 2b and Table A2). In this analysis, mean daily sinking velocities were neither correlated with the amount of sinking particulate organic carbon (POC) nor with the composition of the exported material, including the contribution of biominerals such as biogenic silica and calcium carbonate or the sedimented N:P ratio.

The phytoplankton community succession in the water column was, nevertheless, associated to clear temporal trends in the magnitude and elemental composition of the export flux (Fig. 2a–b). The period of diatom-domination (phase I) was characterized by variable daily fluxes that consisted of almost 30 % biogenic silica. The subsequent shift from diatoms to the dinoflagellate *A. sanguinea* (phase II) was apparent in a five-fold decrease of the opal weight fraction (BSi_{WF}) between t19

https://doi.org/10.5194/egusphere-2022-814
Preprint. Discussion started: 23 August 2022

and t30. Intriguingly, this substantial drop in opal ballast was not reflected by a concomitant decrease in sinking velocities (compare Fig. 2a and 1a–c). During phase II the mean POC_{ST} flux became temporally more stable while it differed substantially between mesocosms, as did the sedimented N:P ratios. The 'orni-eutrophication' in phase III was accompanied by a slight increase in POC_{ST} and a marked increase of TPP_{ST} (see Fig. 7 in Bach et al. 2020) with consequently decreasing sinking matter N:P ratios. All the while, the *A. sanguinea* bloom remained suspended in the water column until the end of the experiment, and did thus probably not contribute much to the sinking flux (Bach et al., 2020).

3.3 Physical particle properties

The physical properties of individual particles were clearly linked to their sinking velocities (Table A3 and Fig. 3b). The most important property was size (ESD), which correlated positively with sinking velocity (see Fig. B2 in the Appendix). Porosity (P_{int}), as the second most influential property, was associated with a decrease in sinking velocity. Particle shape (aspect ratio) on the other hand, had only a comparably minor effect, which was nevertheless still detectable. Rounder particles (high aspect ratio) tended to sink slightly faster than elongated ones. Finally, time (Day) showed the weakest effect here, unlike for the bulk biogeochemical export flux parameters presented before. Altogether, these physical particle properties explained a quarter of the variation in the sinking velocity at the level of the individual particle ($R^2_{marginal}$ = 0.25, Table A3). Whilst we detected interactions between the physical particle properties and time, overarching patterns concerning the development of the relationships over time could not be identified (Fig. B2–4). The variation explained by these interactions was negligible compared to the main effects (Table A3).

Particle size, shape and porosity were relatively similar between mesocosms and OMZ treatments (Fig. 3a). M3 and M4 however, slightly stood out from the rest. During phase II, exported particles in M4 were bigger and more porous compared to the other mesocosms, especially on t30 and t32. M4 also had the highest sinking velocities on t32 in all size classes and among the highest on t30 (Fig. 1a–c). Similarly, in M3 bigger, more porous and slightly more elongated particles sank compared to the other mesocosms. Interestingly, these two mesocosms also showed a distinct phytoplankton community succession. In M4, the community shift from diatoms to dinoflagellates did not happen before the very end of the experiment, while in M3 it occurred ~10 days later than in the other mesocosms (see Fig. 6 in Bach et al. 2020). This is also apparent in the delayed decrease of diatom chlorophyll *a* at around t20 in M3 and M4 (Fig. 1e). The initial diatom communities of M3 and M4 were instead replaced by cryptophytes, and in M4 those were subsequently succeeded by chlorophytes, before *A. sanguinea* finally took over. The deviations in physical particle properties in M3 and M4 might hence be connected to their peculiarities in terms of community succession.

Apart from these two deviations, the median particle size remained relatively stable over time in all mesocosms (Fig. 3a), which implies that the particle size spectrum did not change much throughout the experiment. In contrast, porosities increased slightly and aspect ratios tended to decrease from the beginning to the middle of the experiment (around t30). This

https://doi.org/10.5194/egusphere-2022-814
Preprint. Discussion started: 23 August 2022

implies that particles became less spherical and more porous, which would in theory be associated with decreased sinking velocities. This was reflected relatively well by our data, with decreasing sinking velocities until around t25 (Fig. 1a–c).

4 Discussion

Our mean sinking velocities ranged from 12.8 m d^{-1} in the smallest to 34.2 m d^{-1} in the largest particle size class, which is well in the range of previously published sinking velocities from around the world (size range 40–1000 µm, McDonnell and Buesseler, 2010; Bach et al., 2016, 2019; Iversen and Lampitt, 2020). In Eastern Boundary Upwelling Systems however, direct measurements of sinking velocity are scarce. Reports are restricted to the California Current (Alldredge and Gotschalk, 1988; Ploug et al., 1999) and zooplankton and fish fecal pellets in the Benguela (Ploug et al., 2008) and the Peruvian Upwelling System (Staresinic et al., 1983), respectively.

The sinking rates of aggregates sampled in the Southern California Bight by Ploug et al. (1999) were similar to our largest size fraction (mean ± SD: 31 ± 18 m d^{-1}), although their covered particle size range was significantly larger (~ 1.15 to 6 mm). In the same region, Alldredge and Gotschalk (1988) sampled aggregates that sank more than twice as fast (74 ± 39 m d^{-1}) but also spanned an even larger size range (0.5–25.5 mm). The reported fecal pellets sinking rates were about an order of magnitude higher than our measured sinking velocities. The copepod and appendicularian fecal pellets at Cape Blanc, Mauritania sank at rates of 199 ± 92 and 732 ± 153 m d^{-1}, respectively (Ploug et al., 2008), while the anchovy fecal pellets off the coast of Peru sank at mean rates of 1100 m d^{-1} (691–1987 m d^{-1}, Staresinic et al., 1983). This is not very surprising, as densely packed fecal pellets can reach very high sinking velocities (Steinberg and Landry, 2017). Fischer and Karakas (2009) calculated particle sinking velocities for the Benguela and Canary Current Upwelling Systems by comparing flux data at two different sediment trap sampling depths. Their estimates are high compared to ours (~240 ± 57 m d^{-1} in the Canary Upwelling System and 117 m d^{-1} in the Benguela Upwelling System). However, they covered a different particle size range and it is unclear how well their sediment trap-method compares to our approach.

More comparable to our study are sinking velocity measurements by Cavan et al. (2017) using the same FlowCam method on particles sampled near the coast of Guatemala in the Eastern Tropical North Pacific. Although this system is not an EBUS (Kämpf and Chapman, 2016), it is also characterized by an extensive subsurface oxygen minimum zone (Cavan et al., 2017). The authors measured average sinking velocities of 113.6 m d^{-1} for particles of 489 ± 14 µm size, which is more than three times faster than the 34.2 ± 1.5 m d^{-1} of particles in the 250–1000 µm size range in this study (average size: 420 ± 51.4 µm). Sinking particles in the Peruvian system are thus exposed to more prolonged degradation in the subsurface than those in the Guatemalan region, resulting in increased nitrogen loss through anammox and denitrification (Karthäuser et al., 2021b) and enhanced POC attenuation. It has to be noted, though, that Cavan et al. (2017) collected their particles at greater depths than we did (40–350 m compared to 19 m). As sinking velocities increase with depth due to heterotrophic modifications (Berelson, 2001; Villa-Alfageme et al., 2016), this might be a reason for their higher estimates. Besides, seasonal dynamics

https://doi.org/10.5194/egusphere-2022-814
Preprint. Discussion started: 23 August 2022

and a different state of plankton community succession can cause substantial temporal variability in sinking velocities (e.g. Villa-Alfageme et al., 2016; Bach et al., 2019). The comparison of single measurements from different locations (and depths) should thus be conducted with care. That being said, the sinking velocities of our largest particles were generally low compared to other studies from EBUSs or similar systems.

4.1 Role of phytoplankton community succession and export flux

Due to the time lag between organic matter production and its sinking, it is difficult to analyze the effects of the water column plankton community on the velocity of sinking particles. Therefore, instead of comparing sinking velocities with community composition proxies, we correlated them with export flux parameters, namely the POC flux, sedimented N:P ratio and biogenic mineral fractions (PIC, BSi). These were assessed from bulk sediment trap samples and reflected community composition-related changes in the water column well.

The gradual cease of diatoms and the accompanying decrease in BSi export during phase I was accompanied by decreasing particle sinking velocities in the small and medium size fractions, while at the same time porosities increased (compare Fig. Figure 1, Figure 2 and Figure 3). While diatoms declined, small particles thus became less compact and sank slower. This is somewhat surprising, as particles originating from diatom communities are often relatively porous, slow sinking and inefficient in terms of POC transfer to depth (Lam et al., 2011; Puigcorbé et al., 2015; Bach et al., 2019; Baumann et al., 2021). On the other hand, this finding stands in line with Laurencaeu-Cornec et al. (2020), who found that minerals (calcite in their case) can decrease a particle's porosity. The mechanism is thereby possibly a decrease in stickiness of calcite loaded particles, which can lead to the aggregation of more compact particles (Ball et al., 1987). Perhaps, the same happened here, with non-diatom-derived sinking matter being less opal-rich and more porous, which resulted in slower sinking velocities (see Section 4.2).

The orni-eutrophication at the end of the experiment and the resulting phytoplankton bloom likely induced the strong decrease in sedimented N:P ratios and the noticeable increase in POC export. At the same time, particle porosities decreased and sinking velocities increased in the medium and large size fractions (Fig. B1). The fertilization of the N-depleted system and the consequent export-related changes seem to have affected the properties of sinking particles leading to increased sinking velocities. Interestingly, M4, the mesocosm that differed the most from the others in terms of community composition and succession, did not show an increase in phytoplankton biomass (chlorophyll *a*) during phase III. Yet, the changes in the sedimented N:P ratio and POC flux were similar to the other mesocosms. The reason for this might be that the chlorophyll *a* concentration in M4 was lower than in all other mesocosms during phases II and III. Perhaps, the phytoplankton community was not able to capitalize on the provided nutrients, as opposed to the communities in the other mesocosms. It is conceivable that the bird feces partly sank to the sediment trap directly, instead of fully dissolving in the water column. There, they might have caused the observed shifts in POC and TPP export and particle properties in all mesocosms, including M4, in addition to fueling the overlaying water column productivity in most mesocosms.

https://doi.org/10.5194/egusphere-2022-814
Preprint. Discussion started: 23 August 2022

Another indication for the importance of the community composition dynamics on sinking particle properties lies in the comparison of M3 and M4 to the other mesocosms. Particle sizes and porosities in M3 and especially in M4 were higher than in the other mesocosms during phase II, which was, to a certain degree, reflected by higher sinking velocities. There was a higher contribution of crypto- and chlorophytes in both mesocosms during that time, while the others were dominated by *A. sanguinea* (see Fig. 6 in Bach et al. 2020). At the same time, M4 and especially M3 were among the mesocosms with the highest POC export flux during phase II. This constitutes further evidence for an interaction between the phytoplankton community composition, the resulting export flux and the properties and sinking velocities of settling particles.

4.2 Influence of opal ballast on sinking velocity

We did not find a correlation between mean particle sinking velocities in any size class and the opal weight fraction of the export flux in our experiment. We assume this was due to the relatively small variability in sinking velocity and opal weight fraction between mesocosms on a specific measurement day. In other words, there were no consistent differences between mesocosms on the same day, from which correlations could be detected. Most of the variation occurred over time, which the model attributed to the time effect (factor "Day"). This made the detection of a potential effect of the opal weight fraction difficult. Nonetheless, we would have expected the 5-fold drop in the opal fraction between t18 and t30 to be paralleled by a substantial decrease in sinking velocities. Although mean sinking velocities did initially decrease during this time period, the decrease was relatively moderate (from t18 to t20: 24 %, 27 % and 14 % in the small, medium and large size fraction, respectively) compared to the drop in opal content and sinking velocities remained stable thereafter.

The theoretical effect that a 5-fold drop in the opal weight fraction should have on sinking velocities is substantial. Using Stokes' law (Stokes, 1851), we calculated the effect of different opal ballasting on the sinking velocity of idealized particles. We assumed two spherical particles with 100 µm diameter to consist of POC and BSi exclusively (densities of 1.06 and 2.1 g cm^{-3}, respectively, Klaas and Archer, 2002). One had an opal contribution of 25 %, the other of 5 %, which represents values from before and after the opal drop during phase II. We calculated sinking velocities of 137 and 40 m d^{-1} for the 25 % and 5 % opal particle, respectively. According to this calculation, the observed drop in BSi should have theoretically decreased particle sinking velocities by a factor of 3.4.

One possible explanation could be concurring effects, which changed in parallel with opal ballasting and had opposing (i.e. positive) effects on sinking velocity. Conceivably, there could have been an increase in particle size or compactness due to the phytoplankton community shift or zooplankton repackaging, respectively. However, neither size increased nor porosity decreased while the opal contribution to the export flux declined. On the contrary, porosity even increased in the small and medium particle size classes, mirroring the temporal pattern of the BSi drop (compare Fig. 2a and Fig. B1).

These findings suggest that in a close-to-natural plankton community, the velocities of sinking particles are either not substantially affected by their opal fraction, or other factors balance out its potential influence. This stands in contrast to the "ballast hypothesis", which states that ballasting minerals (opal, calcium carbonate and lithogenic material) enhance the

https://doi.org/10.5194/egusphere-2022-814
Preprint. Discussion started: 23 August 2022

export of organic matter, partly via enhancing particle sinking velocities (Francois et al., 2002; Klaas and Archer, 2002; Armstrong et al., 2002). Although opal is considered a weaker driver of sinking velocity than calcium carbonate, a higher proportion of it should theoretically nonetheless increase sinking velocity (Francois et al., 2002; Klaas and Archer, 2002; Lee et al., 2009; Iversen and Ploug, 2010). Apparently, the idealized opal-sinking velocity relationship does not necessarily hold true in a plankton community in the surface ocean. The reason for this is likely the complexity of pelagic systems, in which numerous physical and biological drivers affect particle sinking velocities, such as size and porosity, particle type (McDonnell and Buesseler, 2010; Durkin et al., 2021), phytoplankton community composition via porosity and ballasting (e.g. Bach et al., 2016, 2019) or even diatom morphology (Laurenceau-Cornec et al., 2015). To disentangle this multitude of mechanisms, targeted laboratory studies are needed. Thus far however, most such studies have compared sinking velocities of aggregates formed by different algae species (e.g. Iversen and Ploug, 2010) without gaining much insight into the mechanistic relationships between sinking velocity and its individual drivers. In order to better resolve the relationship between sinking velocity and opal ballasting, a study similar to the one by Laurenceau-Cornec et al. (2020) is needed, who designed an experiment specifically to examine effects of calcite ballasting on particle sinking velocities.

4.3 Size, porosity and shape as drivers of sinking velocity

We found that among our tested physical particle properties, size had the strongest correlation with sinking velocity. This stands in contrast to a recent study, which did not detect a relationship between size and sinking velocity (Iversen and Lampitt, 2020). One reason for this might be that the effect size is small, thus requiring a large test power to detect it. While our study found a rather small effect size (partial effect size: $\eta_p^2 = 0.16$, Table A3) encompassing measurements of more than a hundred thousand particles, Iversen and Lampitt (2020) measured a total of 1060 particles, which was perhaps insufficient to detect a correlation. Another reason might be that they measured their particles *in situ*, in contrast to our *ex situ* measurement method. Williams and Giering (2022) recently argued that sampling marine particles can modify, damage and disaggregate them, which might cause the particle pool to become more homogeneous than in the natural environment and strengthen the relationship between particle size and sinking velocity. Finally, the size-sinking relationship is subject to large temporal and spatial variability, which is why the importance for location-specific estimates for it has often been highlighted (Laurenceau-Cornec et al., 2015; Giering et al., 2020; Cael et al., 2021). We estimated such a relationship for our data set in order to provide the first empirical size-sinking-relationship for particles from the Peruvian Upwelling System (Fig. 4). Our average estimates for the scaling factors α and β were well in range of Cael et al.'s estimates (2021, see their Figures 3 and 4) and might thus help modelers to optimize local particle flux parameterizations for the Peruvian Upwelling System.

Particle porosity was the second most important driver of sinking velocity. Surprisingly, the correlation between sinking velocity and porosity was three times weaker than the one with size. So although porosity has repeatedly been reported as an important driver of sinking velocity (Alldredge and Crocker, 1995; Giering et al., 2020; Laurenceau-Cornec et al., 2020), it seems that in the size range of 40–1000 µm particle size is the more influential property. Our study is, to the best of our

https://doi.org/10.5194/egusphere-2022-814
Preprint. Discussion started: 23 August 2022

knowledge, the first to directly compare the size-sinking and porosity-sinking relationships in a marine particle dataset, providing insight into the relative importance of these two drivers on sinking velocity.

The third assessed particle property, shape, was inconsequential compared to the former two, both in comparison and in absolute terms. Although rounder particles tended to sink faster than elongated ones, the aspect ratio was not overly important in driving sinking velocities. Although particle shape has been found to influence the sinking behavior (e.g. Laurenceau-Cornec et al., 2015, 2020), it is not considered as important a driver as particle size or compactness. Our results concur with this, indicating that although the aspect ratio of a particle matters, it is not a major driver of sinking velocity. Multiple times more important seem to be porosity and size, with size being the predominant driver.

5 Conclusions

We provide the first empirical data on particle sinking velocities in the small to medium size range (40–1000 µm) in the coastal Peruvian Upwelling System. Our data fit relatively well into the range of previously published estimates of equally-sized particles from around the world. However, particles in our largest size fraction (~0.4 mm diameter) sank slower than those in some other EBUSs and comparable systems.

We found indications that sinking velocities were connected to the phytoplankton community composition and succession and to the nutritional system status. Which species make up the base of the food web in the Peruvian Upwelling System seems to influence how fast particles sink and hence how much POC is remineralized in the subsurface OMZ. Our results further show that when a system shifts away from a diatom-based community, opal ballast does not seem to be a major driver of sinking velocity in the surface ocean. In order to disentangle the mechanisms driving particle sinking velocity under such a community shift, laboratory studies are needed that can isolate the effects of the potential drivers such as opal ballast, particle size and compactness.

Our results suggest that sinking velocity parameterizations in numerical models should include particle size and porosity as physical particle properties, with size as the more influential driver. The provided metrics of a size-sinking relationship could help to further optimize local particle flux parameterizations. Since sinking velocity determines for how long particles are exposed to degradation processes on their way to depth, it is a crucial parameter for assessing carbon sequestration and changes in subsurface oxygen concentrations. This is especially important for a region that is highly susceptible to climate-driven changes. Our study might thus help to better estimate the strength and efficiency of the biological carbon pump in the Peruvian Upwelling System and hence project the expansion of the local oxygen-deficient waters.

https://doi.org/10.5194/egusphere-2022-814
Preprint. Discussion started: 23 August 2022

Appendix A: Tables

Response variable	Source of variation	df	MS	F-value	$R^2_{marginal}$	p-value
a) Sinking velocity 40–100µm	OMZ	1	0.065	0.02	0.42	0.904
	Day	18	20.172	4.93		**<0.0001**
	OMZ × Day	18	4.702	1.15		0.318
b) log10(sinking velocity 100–250µm)	OMZ	1	0.006	0.67	0.42	0.416
	Day	18	0.040	4.74		**<0.0001**
	OMZ × Day	18	0.008	1.00		0.465
c) log10(sinking velocity 250–1000µm)	OMZ	1	0.004	0.34	0.48	0.559
	Day	18	0.070	6.07		**<0.0001**
	OMZ × Day	18	0.012	1.08		0.383

Table A1. Linear mixed models for the effects of oxygen minimum zone (OMZ) treatment across time on averaged sinking velocity per size class. Shown are the ANOVA output (df: degrees of freedom, MS: mean squares), R^2 of fixed effects ($R^2_{marginal}$) and partial effect sizes (η_p^2). Measurement days before the OMZ water addition (sampling days t2–t10) were excluded. Model diagnostics: Raw data of a) met the assumptions for normality and homogeneity. For b) and c) the response variable was log10-transformed to meet the assumptions for normality and homogeneity.

Response variable	Source of variation	df	MS	F-value	η_p^2	$R^2_{marginal}$	p-value
a) Sinking velocity 40–100 µm	Day	23	29.971	5.27	0.436	0.50	**<0.0001**
	BSi_{WF}	1	1.730	0.30	0.001		0.582
	PIC_{WF}	1	0.412	0.07	0.000		0.788
	POC_{ST}	1	7.624	1.34	0.005		0.249
	N_{ST}:P_{ST}	1	0.279	0.05	0.000		0.825
b) log10(sinking velocity 100–250 µm)	Day	23	0.020	2.29	0.246	0.39	**0.002**
	BSi_{WF}	1	0.014	1.64	0.008		0.202
	PIC_{WF}	1	0.000	0.03	0.000		0.866

https://doi.org/10.5194/egusphere-2022-814
Preprint. Discussion started: 23 August 2022

	POC_{ST}	1	0.007	0.84	0.004		0.361
	N_{ST}:P_{ST}	1	0.000	0.03	0.000		0.871
c) log10(sinking velocity 250–1000 µm)	Day	23	0.036	2.88	0.300	0.41	**<0.0001**
	BSi_{WF}	1	0.000	0.02	0.000		0.884
	PIC_{WF}	1	0.002	0.17	0.001		0.682
	POC_{ST}	1	0.043	3.43	0.015		0.066
	N_{ST}:P_{ST}	1	0.001	0.06	0.000		0.811

Table A2. Linear mixed models for the relationships between averaged sinking velocities per size class and biogeochemical particle properties and time. Shown are the ANOVA output (df: degrees of freedom, MS: mean squares), R^2 of fixed effects ($R^2_{marginal}$) and partial effect sizes (η_p^2). Model diagnostics: Raw data of a) met the assumptions for normality and homogeneity. For b) and c) the response variable was log10-transformed to meet the assumptions for normality and homogeneity.

Response variable	Source of variation	df	MS	F-value	η_p^2	$R^2_{marginal}$	p-value
log10(sinking velocity)	log10(ESD)	1	1274.95	19500.45	0.160	0.25	**<0.0001**
	log10(P_{int})	1	368.41	5634.81	0.052		**<0.0001**
	Aspect Ratio	1	28.05	429.10	0.004		**<0.0001**
	Day	23	0.51	7.77	0.002		**<0.0001**
	log10(ESD) × Day	23	0.51	7.83	0.002		**<0.0001**
	log10(P_{int}) × Day	23	0.52	7.99	0.002		**<0.0001**
	Aspect Ratio × Day	23	1.25	19.06	0.004		**<0.0001**

Table A3. Linear mixed models for the relationships between sinking velocity and physical particle properties (size, porosity and shape) across time. Shown are the ANOVA output (df: degrees of freedom, MS: mean squares), R^2 of fixed effects ($R^2_{marginal}$) and partial effect sizes (η_p^2). The analysis is based on N > 100,000 particles. Model diagnostics: The right-skewed sinking velocity, ESD and P_{int} data were log10-transformed, after which only slight deviations from normality remained. Particles within one measurement were correlated with each other. The reason might be that fast sinking particles were generally measured at the beginning of a measurement, while more slow particles were measured towards the end. We nevertheless argue that our model results are interpretable due to the high significance of our correlations (all p-values < 10^{-24}).

https://doi.org/10.5194/egusphere-2022-814
Preprint. Discussion started: 23 August 2022

Appendix B: Figures

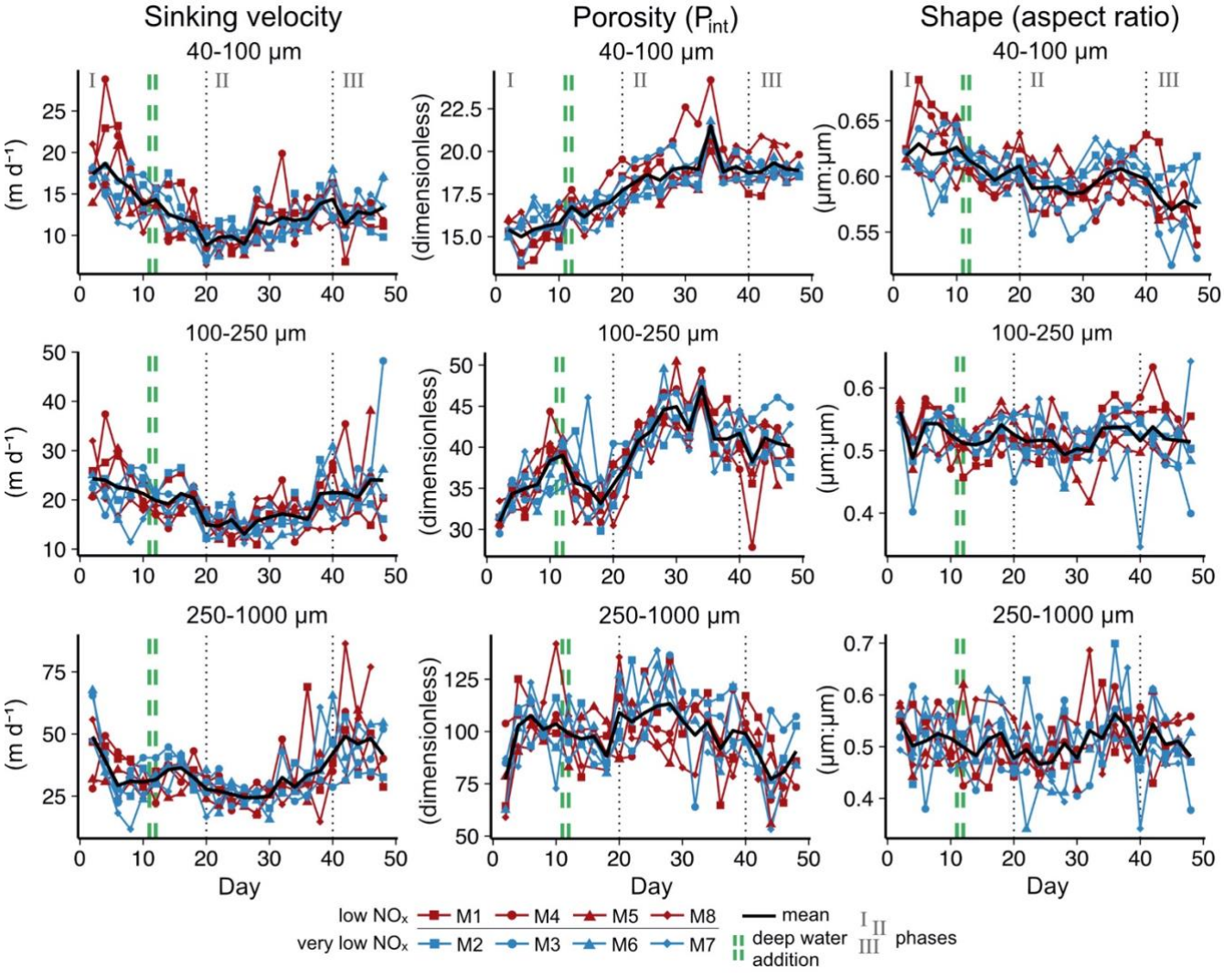

Figure B1. Temporal developments of particle sinking velocities, porosities and shapes per size class. Note that sinking velocities are also shown in Fig. 1, but are replicated here to facilitate the comparison with other particle properties.

https://doi.org/10.5194/egusphere-2022-814
Preprint. Discussion started: 23 August 2022

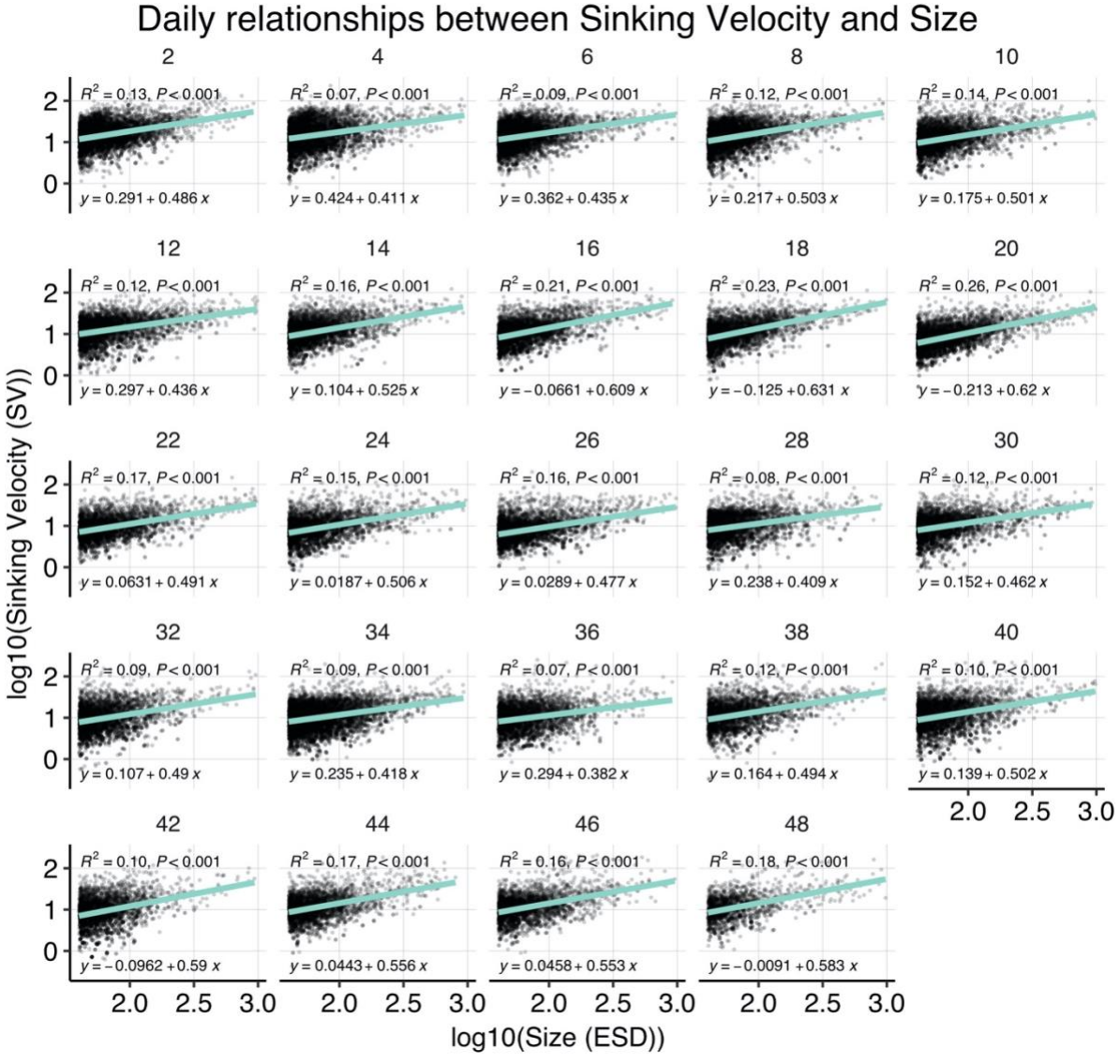

Figure B2. Correlations between sinking velocity and particle size over time. Each panel shows data of all mesocosms for one experimental day, including a linear regression with test statistics and model formula, and each black dot corresponds to one particle. Related model output: Table A3 and Fig. 3b.

https://doi.org/10.5194/egusphere-2022-814
Preprint. Discussion started: 23 August 2022

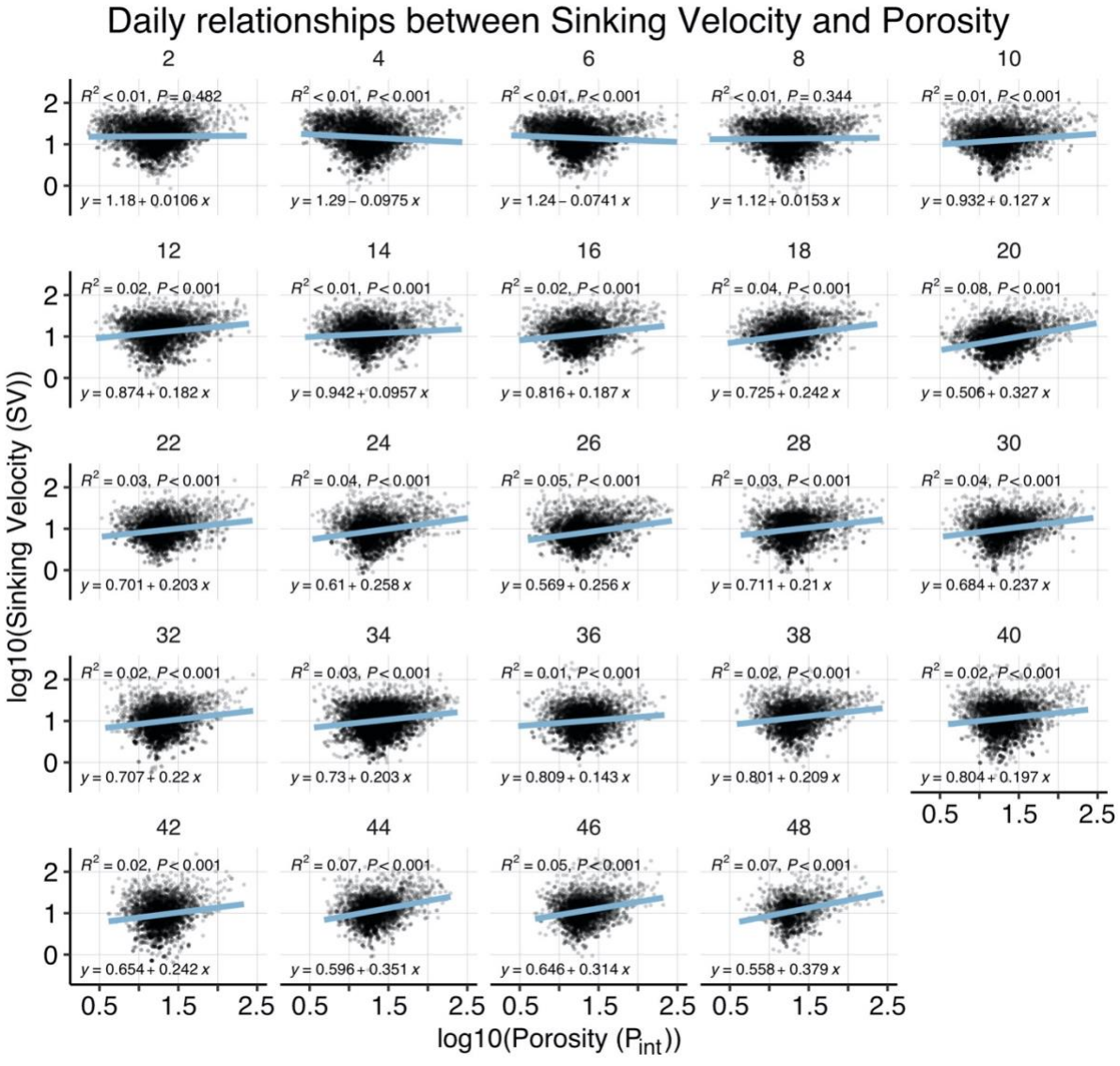

Figure B3. Correlations between sinking velocity and particle porosity over time. Each panel shows data of all mesocosms for one experimental day, including a linear regression with test statistics and model formula. Related model output: Table A3 and Fig. 3b.

https://doi.org/10.5194/egusphere-2022-814
Preprint. Discussion started: 23 August 2022

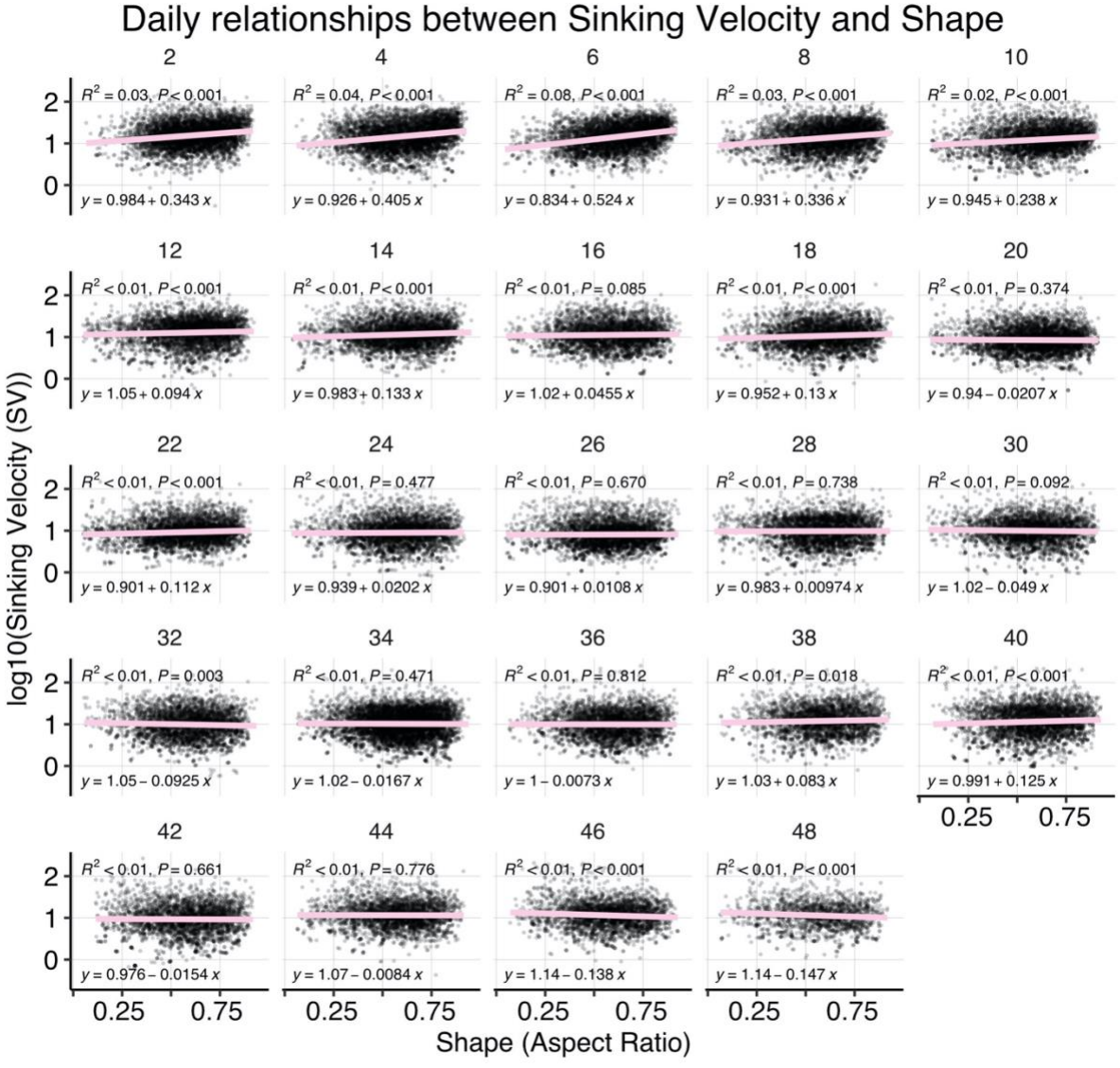

Figure B4. Correlations between sinking velocity and particle size over time. Each panel shows data of all mesocosms for one experimental day, including a linear regression with test statistics and model formula. Related model output: Table A3 and Fig. 3b.

Data availability. The data shown in this study will soon be available on PANGAEA.

Author contributions. LTB, AJP and UR designed the experiment. PS, LTB, FM, AJP and UR contributed to the sampling. MB, LTB, SG, AJP and JT analyzed the data. MB wrote the manuscript with comments from all co-authors.

Competing interests. The authors declare that the research was conducted in the absence of any commercial or financial relationships that could be construed as a potential conflict of interest.

https://doi.org/10.5194/egusphere-2022-814
Preprint. Discussion started: 23 August 2022

Special issue statement. This article is part of the special issue "Ecological and biogeochemical functioning of the coastal upwelling system off Peru: an in situ mesocosm study". It is not associated with a conference.

Acknowledgements. We thank all the participants of the KOSMOS Peru 2017 study for their efforts in mesocosm sampling and maintenance. We want to thank in particular Dr. Paul Stange for conducting the particle sinking velocity measurements and Fabrizio Minutolo and Dr. Tim Boxhammer for the biogeochemical sampling and processing of the sediment trap material. The employees of the IMARPE institute deserve a special thanks for all kinds of support they have provided us with during the planning, preparation and execution of this study. We are also thankful to Club Náutico del Centro Naval for hosting part of our laboratories and offices. This work has been carried out in the framework of the cooperation agreement between IMARPE and GEOMAR through the German Federal Ministry of Education and Research (BMBF) project ASLAEL 12-016 and the national project Integrated Study of the Upwelling System off Peru developed by the Directorate of Oceanography and Climate Change of IMARPE, PPR 137 CONCYTEC.

Financial support. This study was funded by the Collaborative Research Center SFB 754 Climate-Biogeochemistry Interactions in the Tropical Ocean financed by the German Research Foundation (DFG). Additional funds were provided by the EU project AQUACOSM via the European Union's Horizon 2020 research and innovation program under grand agreement No 731065 and through the Leibniz Award 2012, granted to Ulf Riebesell.

References

Alldredge, A. L. and Crocker, K. M.: Why do sinking mucilage aggregates accumulate in the water column?, Science of The Total Environment, 165, 15–22, https://doi.org/10.1016/0048-9697(95)04539-D, 1995.

Alldredge, A. L. and Gotschalk, C.: In situ settling behavior of marine snow, Limnol. Oceanogr., 33, 339–351, https://doi.org/10.4319/lo.1988.33.3.0339, 1988.

Armstrong, R. A., Lee, C., Hedges, J. I., Honjo, S., and Wakeham, S. G.: A new, mechanistic model for organic carbon fluxes in the ocean based on the quantitative association of POC with ballast minerals, Deep-sea Research Part Ii-topical Studies in Oceanography, https://doi.org/10.1016/s0967-0645(01)00101-1, 2002.

Armstrong, R. A., Peterson, M. L., Lee, C., and Wakeham, S. G.: Settling velocity spectra and the ballast ratio hypothesis, Deep Sea Research Part II: Topical Studies in Oceanography, 56, 1470–1478, https://doi.org/10.1016/j.dsr2.2008.11.032, 2009.

Bach, L. T., Riebesell, U., Sett, S., Febiri, S., Rzepka, P., and Schulz, K. G.: An approach for particle sinking velocity measurements in the 3–400 µm size range and considerations on the effect of temperature on sinking rates, Mar Biol, 159, 1853–1864, https://doi.org/10.1007/s00227-012-1945-2, 2012.

Bach, L. T., Boxhammer, T., Larsen, A., Hildebrandt, N., Schulz, K. G., and Riebesell, U.: Influence of plankton community structure on the sinking velocity of marine aggregates: Sinking velocity of marine aggregates, Global Biogeochem. Cycles, 30, 1145–1165, https://doi.org/10.1002/2016GB005372, 2016.

https://doi.org/10.5194/egusphere-2022-814
Preprint. Discussion started: 23 August 2022

Bach, L. T., Stange, P., Taucher, J., Achterberg, E. P., Algueró-Muñiz, M., Horn, H., Esposito, M., and Riebesell, U.: The Influence of Plankton Community Structure on Sinking Velocity and Remineralization Rate of Marine Aggregates, Global Biogeochem. Cycles, 33, 971–994, https://doi.org/10.1029/2019GB006256, 2019.

Bach, L. T., Paul, A. J., Boxhammer, T., von der Esch, E., Graco, M., Schulz, K. G., Achterberg, E., Aguayo, P., Arístegui, J., Ayón, P., Baños, I., Bernales, A., Boegeholz, A. S., Chavez, F., Chavez, G., Chen, S.-M., Doering, K., Filella, A., Fischer, M., Grasse, P., Haunost, M., Hennke, J., Hernández-Hernández, N., Hopwood, M., Igarza, M., Kalter, V., Kittu, L., Kohnert, P., Ledesma, J., Lieberum, C., Lischka, S., Löscher, C., Ludwig, A., Mendoza, U., Meyer, J., Meyer, J., Minutolo, F., Ortiz Cortes, J., Piiparinen, J., Sforna, C., Spilling, K., Sanchez, S., Spisla, C., Sswat, M., Zavala Moreira, M., and Riebesell, U.: Factors controlling plankton community production, export flux, and particulate matter stoichiometry in the coastal upwelling system off Peru, Biogeosciences, 17, 4831–4852, https://doi.org/10.5194/bg-17-4831-2020, 2020.

Ball, R. C., Weitz, D. A., Witten, T. A., and Leyvraz, F.: Universal kinetics in reaction-limited aggregation, Phys. Rev. Lett., 58, 274–277, https://doi.org/10.1103/PhysRevLett.58.274, 1987.

Barlow, R. G., Cummings, D. G., and Gibb, S. W.: Improved resolution of mono- and divinyl chlorophylls a and b and zeaxanthin and lutein in phytoplankton extracts using reverse phase C-8 HPLC, Marine Ecology Progress Series, 161, 303–307, https://doi.org/10.3354/meps161303, 1997.

Bates, D., Mächler, M., Bolker, B., and Walker, S.: Fitting Linear Mixed-Effects Models Using **lme4**, J. Stat. Soft., 67, https://doi.org/10.18637/jss.v067.i01, 2015.

Baumann, M., Taucher, J., Paul, A. J., Heinemann, M., Vanharanta, M., Bach, L. T., Spilling, K., Ortiz, J., Arístegui, J., Hernández-Hernández, N., Baños, I., and Riebesell, U.: Effect of Intensity and Mode of Artificial Upwelling on Particle Flux and Carbon Export, Front. Mar. Sci., 8, 742142, https://doi.org/10.3389/fmars.2021.742142, 2021.

Berelson, W. M.: Particle settling rates increase with depth in the ocean, Deep-sea Research Part Ii-topical Studies in Oceanography, https://doi.org/10.1016/s0967-0645(01)00102-3, 2001.

Boxhammer, T., Bach, L. T., Czerny, J., and Riebesell, U.: Technical note: Sampling and processing of mesocosm sediment trap material for quantitative biogeochemical analysis, Biogeosciences, 13, 2849–2858, https://doi.org/10.5194/bg-13-2849-2016, 2016.

Cael, B. B., Cavan, E. L., and Britten, G. L.: Reconciling the Size-Dependence of Marine Particle Sinking Speed, Geophys Res Lett, 48, https://doi.org/10.1029/2020GL091771, 2021.

Cavan, E. L., Trimmer, M., Shelley, F., and Sanders, R.: Remineralization of particulate organic carbon in an ocean oxygen minimum zone, Nat Commun, 8, 14847, https://doi.org/10.1038/ncomms14847, 2017.

Chavez, F. P. and Messié, M.: A comparison of Eastern Boundary Upwelling Ecosystems, Progress in Oceanography, 83, 80–96, https://doi.org/10.1016/j.pocean.2009.07.032, 2009.

DiTullio, G. R., Geesey, M. E., Maucher, J. M., Alm, M. B., Riseman, S. F., and Bruland, K. W.: Influence of iron on algal community composition and physiological status in the Peru upwelling system, Limnology and Oceanography, 50, 1887–1907, https://doi.org/10.4319/lo.2005.50.6.1887, 2005.

Durkin, C. A., Buesseler, K. O., Cetinić, I., Estapa, M. L., Kelly, R. P., and Omand, M. M.: A Visual Tour of Carbon Export by Sinking Particles, Global Biogeochemical Cycles, https://doi.org/10.1029/2021gb006985, 2021.

https://doi.org/10.5194/egusphere-2022-814
Preprint. Discussion started: 23 August 2022

Fischer, G. and Karakas, G.: Sinking rates and ballast composition of particles in the Atlantic Ocean: implications for the organic carbon fluxes to the deep ocean, Biogeosciences, https://doi.org/10.5194/bg-6-85-2009, 2009.

Francois, R., Honjo, S., Krishfield, R., and Manganini, S.: Factors controlling the flux of organic carbon to the bathypelagic zone of the ocean: Factors controlling organic carbon flux, Global Biogeochem. Cycles, 16, 34-1-34–20, https://doi.org/10.1029/2001GB001722, 2002.

Giering, S. L. C., Cavan, E. L., Basedow, S. L., Briggs, N., Burd, A. B., Darroch, L. J., Guidi, L., Irisson, J.-O., Iversen, M. H., Kiko, R., Lindsay, D., Marcolin, C. R., McDonnell, A. M. P., Möller, K. O., Passow, U., Thomalla, S., Trull, T. W., and Waite, A. M.: Sinking Organic Particles in the Ocean—Flux Estimates From in situ Optical Devices, Front. Mar. Sci., 6, 834, https://doi.org/10.3389/fmars.2019.00834, 2020.

Guidi, L., Stemmann, L., Jackson, G. A., Ibanez, F., Claustre, H., Legendre, L., Picheral, M., and Gorskya, G.: Effects of phytoplankton community on production, size, and export of large aggregates: A world-ocean analysis, Limnol. Oceanogr., 54, 1951–1963, https://doi.org/10.4319/lo.2009.54.6.1951, 2009.

Hansen, H. P. and Koroleff, F.: Determination of nutrients, in: Methods of Seawater Analysis, Third, Completely Revised and Extended Edition, WILEY-VCH, 159–228, 1999.

Iversen, M. H. and Lampitt, R. S.: Size does not matter after all: No evidence for a size-sinking relationship for marine snow, Progress in Oceanography, https://doi.org/10.1016/j.pocean.2020.102445, 2020.

Iversen, M. H. and Ploug, H.: Ballast minerals and the sinking carbon flux in the ocean: carbon-specific respiration rates and sinking velocity of marine snow aggregates, Biogeosciences, 7, 2613–2624, https://doi.org/10.5194/bg-7-2613-2010, 2010.

Kalvelage, T., Lavik, G., Lam, P., Contreras, S., Arteaga, L., Löscher, C. R., Oschlies, A., Paulmier, A., Stramma, L., and Kuypers, M. M. M.: Nitrogen cycling driven by organic matter export in the South Pacific oxygen minimum zone, https://doi.org/10.1594/pangaea.843461, 2013.

Kämpf, J. and Chapman, P.: Upwelling Systems of the World, Springer International Publishing, Cham, 433 pp., https://doi.org/10.1007/978-3-319-42524-5, 2016.

Karstensen, J., Stramma, L., and Visbeck, M.: Oxygen minimum zones in the eastern tropical Atlantic and Pacific oceans, Progress in Oceanography, 77, 331–350, https://doi.org/10.1016/j.pocean.2007.05.009, 2008.

Karthäuser, C., Ahmerkamp, S., Marchant, H. K., Bristow, L. A., Hauss, H., Iversen, M. H., Kiko, R., Maerz, J., Lavik, G., and Kuypers, M. M. M.: Small sinking particles control anammox rates in the Peruvian oxygen minimum zone., Nature Communications, https://doi.org/10.1038/s41467-021-23340-4, 2021a.

Karthäuser, C., Ahmerkamp, S., Marchant, H. K., Bristow, L. A., Hauss, H., Iversen, M. H., Kiko, R., Maerz, J., Lavik, G., and Kuypers, M. M. M.: Small sinking particles control anammox rates in the Peruvian oxygen minimum zone., Nature Communications, https://doi.org/10.1038/s41467-021-23340-4, 2021b.

Khatiwala, S., Tanhua, T., Mikaloff Fletcher, S., Gerber, M., Doney, S. C., Graven, H. D., Gruber, N., McKinley, G. A., Murata, A., Ríos, A. F., and Sabine, C. L.: Global ocean storage of anthropogenic carbon, Biogeosciences, 10, 2169–2191, https://doi.org/10.5194/bg-10-2169-2013, 2013.

Klaas, C. and Archer, D.: Association of sinking organic matter with various types of mineral ballast in the deep sea: Implications for the rain ratio, Global Biogeochemical Cycles, https://doi.org/10.1029/2001gb001765, 2002.

https://doi.org/10.5194/egusphere-2022-814
Preprint. Discussion started: 23 August 2022

Kuznetsova, A., Brockhoff, P. B., and Christensen, R. H. B.: lmerTest Package: Tests in Linear Mixed Effects Models, J. Stat. Soft., 82, https://doi.org/10.18637/jss.v082.i13, 2017.

Lam, P. J., Doney, S. C., and Bishop, J. K. B.: The dynamic ocean biological pump: Insights from a global compilation of particulate organic carbon, $CaCO_3$, and opal concentration profiles from the mesopelagic: The dynamic ocean biological pump, Global Biogeochem. Cycles, 25, n/a-n/a, https://doi.org/10.1029/2010GB003868, 2011.

Laurenceau-Cornec, E. C., Trull, T. W., Davies, D. M., Bray, S. G., Doran, J., Planchon, F., Carlotti, F., Jouandet, M.-P., Cavagna, A.-J., Waite, A. M., and Blain, S.: The relative importance of phytoplankton aggregates and zooplankton fecal pellets to carbon export: insights from free-drifting sediment trap deployments in naturally iron-fertilised waters near the Kerguelen Plateau, Biogeosciences, 12, 1007–1027, https://doi.org/10.5194/bg-12-1007-2015, 2015.

Laurenceau-Cornec, E. C., Le Moigne, F. A. C., Gallinari, M., Moriceau, B., Toullec, J., Iversen, M. H., Engel, A., and De La Rocha, C. L.: New guidelines for the application of Stokes' models to the sinking velocity of marine aggregates, Limnology and Oceanography, 65, 1264–1285, https://doi.org/10.1002/lno.11388, 2020.

Lee, C., Peterson, M. L., Wakeham, S. G., Armstrong, R. A., Cochran, J. K., Miquel, J. C., Fowler, S. W., Hirschberg, D., Beck, A., and Xue, J.: Particulate organic matter and ballast fluxes measured using time-series and settling velocity sediment traps in the northwestern Mediterranean Sea, Deep Sea Research Part II: Topical Studies in Oceanography, 56, 1420–1436, https://doi.org/10.1016/j.dsr2.2008.11.029, 2009.

Lüdecke, D.: Statistical Functions for Regression Models (Version 0.18.1), https://doi.org/10.5281/zenodo.1284472, n.d.

Lüdecke, D., Ben-Shachar, M., Patil, I., Waggoner, P., and Makowski, D.: performance: An R Package for Assessment, Comparison and Testing of Statistical Models, JOSS, 6, 3139, https://doi.org/10.21105/joss.03139, 2021.

Mackey, M. D., Mackey, D. J., Higgins, H. W., and Wright, S. W.: CHEMTAX - a program for estimating class abundances from chemical markers: application to HPLC measurements of phytoplankton, Marine Ecology Progress Series, 144, 265–283, https://doi.org/10.3354/meps144265, 1996.

Marsay, C. M., Sanders, R. J., Henson, S. A., Pabortsava, K., Achterberg, E. P., and Lampitt, R. S.: Attenuation of sinking particulate organic carbon flux through the mesopelagic ocean, Proc. Natl. Acad. Sci. U.S.A., 112, 1089–1094, https://doi.org/10.1073/pnas.1415311112, 2015.

McDonnell, A. M. P. and Buesseler, K. O.: Variability in the average sinking velocity of marine particles, Limnol. Oceanogr., 55, 2085–2096, https://doi.org/10.4319/lo.2010.55.5.2085, 2010.

McDonnell, A. M. P., Boyd, P. W., and Buesseler, K. O.: Effects of sinking velocities and microbial respiration rates on the attenuation of particulate carbon fluxes through the mesopelagic zone, Global Biogeochemical Cycles, https://doi.org/10.1002/2014gb004935, 2015.

Paul, A. P., Bach, L. T., Schulz, K. G., Boxhammer, T., Czerny, J., Achterberg, E. P., Hellemann, D., Trense, Y., Nausch, M., Sswat, M., and Riebesell, U.: Effect of elevated CO_2 on organic matter pools and fluxes in a summer Baltic Sea plankton community, Biogeosciences, 12, 6181–6203, https://doi.org/10.5194/bg-12-6181-2015, 2015.

Pennington, J. T., Mahoney, K. L., Kuwahara, V. S., Kolber, D. D., Calienes, R., and Chavez, F. P.: Primary production in the eastern tropical Pacific: A review, Progress in Oceanography, https://doi.org/10.1016/j.pocean.2006.03.012, 2006.

https://doi.org/10.5194/egusphere-2022-814
Preprint. Discussion started: 23 August 2022

Ploug, H., Grossart, H.-P., Azam, F., and Jørgensen, B. B.: Photosynthesis, respiration, and carbon turnover in sinking marine snow from surface waters of Southern California Bight: implications for the carbon cycle in the ocean., Marine Ecology Progress Series, https://doi.org/10.3354/meps179001, 1999.

Ploug, H., Iversen, M. H., and Fischer, G.: Ballast, sinking velocity, and apparent diffusivity within marine snow and zooplankton fecal pellets: Implications for substrate turnover by attached bacteria, Limnology and Oceanography, https://doi.org/10.4319/lo.2008.53.5.1878, 2008.

Puigcorbé, V., Benitez-Nelson, C. R., Masqué, P., Verdeny, E., White, A. E., Popp, B. N., Prahl, F. G., and Lam, P. J.: Small phytoplankton drive high summertime carbon and nutrient export in the Gulf of California and Eastern Tropical North Pacific, Global Biogeochem. Cycles, 29, 1309–1332, https://doi.org/10.1002/2015GB005134, 2015.

R Core Team: R: A Language and Environment for Statistical Computing, 2021.

Riebesell, U., Czerny, J., von Bröckel, K., Boxhammer, T., Büdenbender, J., Deckelnick, M., Fischer, M., Hoffmann, D., Krug, S. A., Lentz, U., Ludwig, A., Muche, R., and Schulz, K. G.: Technical Note: A mobile sea-going mesocosm system – new opportunities for ocean change research, Biogeosciences, 10, 1835–1847, https://doi.org/10.5194/bg-10-1835-2013, 2013.

Riley, J. S., Sanders, R., Marsay, C. M., Le Moigne, F. A. C., Achterberg, E. P., and Poulton, A. J.: The relative contribution of fast and slow sinking particles to ocean carbon export, Global Biogeochemical Cycles, https://doi.org/10.1029/2011gb004085, 2012.

Ristow, G. H.: Wall correction factor for sinking cylinders in fluids, Phys. Rev. E, 55, 2808–2813, https://doi.org/10.1103/PhysRevE.55.2808, 1997.

Sharp, J. H.: Improved analysis for "particulate" organic carbon and nitrogen from seawater, Limnol. Oceanogr., 19, 984–989, https://doi.org/10.4319/lo.1974.19.6.0984, 1974.

Smetacek, V., Klaas, C., Strass, V., Assmy, P., Montresor, M., Cisewski, B., Savoye, N., Webb, A., d'Ovidio, F., Arrieta, J. M., Bathmann, U., Bellerby, R. G. J., Berg, G. M., Croot, P., Gonzalez, S. F., Henjes, J., Herndl, G. J., Hoffmann, L. J., Leach, H., Losch, M., Mills, M. M., Neill, C., Peeken, I., Röttgers, R., Sachs, O., Sauter, E., Schmidt, M. M., Schwarz, J. N., Terbrüggen, A., and Wolf-Gladrow, D.: Deep carbon export from a Southern Ocean iron-fertilized diatom bloom, Nature, 487, 313–319, https://doi.org/10.1038/nature11229, 2012.

Staresinic, N., Farrington, J. W., Gagosian, R. B., Clifford, C. H., and Hulburt, E. M.: Downward Transport of Particulate Matter in the Peru Coastal Upwelling: Role of the Anchoveta, Engraulis Ringens, https://doi.org/10.1007/978-1-4615-6651-9_12, 1983.

Steinberg, D. K. and Landry, M. R.: Zooplankton and the Ocean Carbon Cycle, Annu. Rev. Mar. Sci., 9, 413–444, https://doi.org/10.1146/annurev-marine-010814-015924, 2017.

Stokes, G. G.: On the Effect of the Internal Friction of Fluids on the Motion of Pendulums, Transactions of the Cambridge Philosophical Society, 9, 8–106, 1851.

Turner, J. T.: Zooplankton fecal pellets, marine snow, phytodetritus and the ocean's biological pump, Progress in Oceanography, 130, 205–248, https://doi.org/10.1016/j.pocean.2014.08.005, 2015.

https://doi.org/10.5194/egusphere-2022-814
Preprint. Discussion started: 23 August 2022

Villa-Alfageme, M., de Soto, F. C., Ceballos, E., Giering, S. L. C., Le Moigne, F. A. C., Henson, S., Mas, J. L., and Sanders, R. J.: Geographical, seasonal, and depth variation in sinking particle speeds in the North Atlantic, Geophys. Res. Lett., 43, 8609–8616, https://doi.org/10.1002/2016GL069233, 2016.

Wickham, H., Averick, M., Bryan, J., Chang, W., D'Agostino McGowan, L., François, R., Grolemund, G., Hayes, A., Henry, L., Hester, J., Kuhn, M., Pedersen, T. L., Miller, E., Bache, S. M., Müller, K., Ooms, J., Robinson, D., Seidel, D. P., Spinu, V., Takahashi, K., Vaughan, D., Wilke, C., Woo, K., and Hiroaki, Y.: Welcome to the tidyverse, Journal of Open Source Software, 4, 1686, https://doi.org/10.21105/joss.01686, 2019.

Williams, J. R. and Giering, S. L. C.: In situ Particle Measurements Deemphasize the Role of Size in Governing Particle Sinking Velocity, Oceanography, https://doi.org/10.1002/essoar.10511459.1, 2022.

Figures

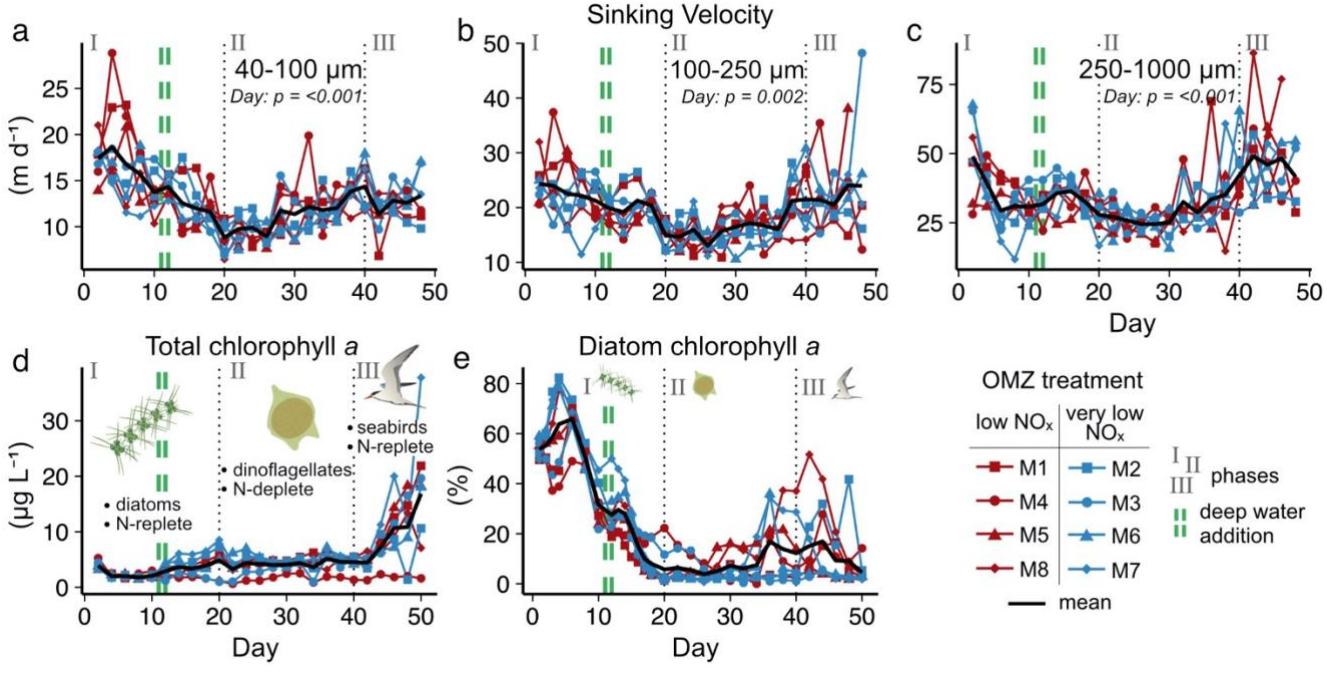

Figure 1. Temporal developments in particle sinking velocities and phytoplankton community. (**a**)–(**c**) Mean daily sinking velocities sampled from the sediment trap in three particle size classes. Significant fixed effects (*OMZ*, *Day* or *OMZ*×*Day*) are displayed including p-values (Table A1). (**d**)–(**e**) Total chlorophyll *a* and the contribution of diatoms to total chlorophyll *a* in the water column. Here, the shifts in phytoplankton and trophic state are indicated by text and symbols (Integration and Application Network; ian.umces.edu/media-library).

https://doi.org/10.5194/egusphere-2022-814
Preprint. Discussion started: 23 August 2022

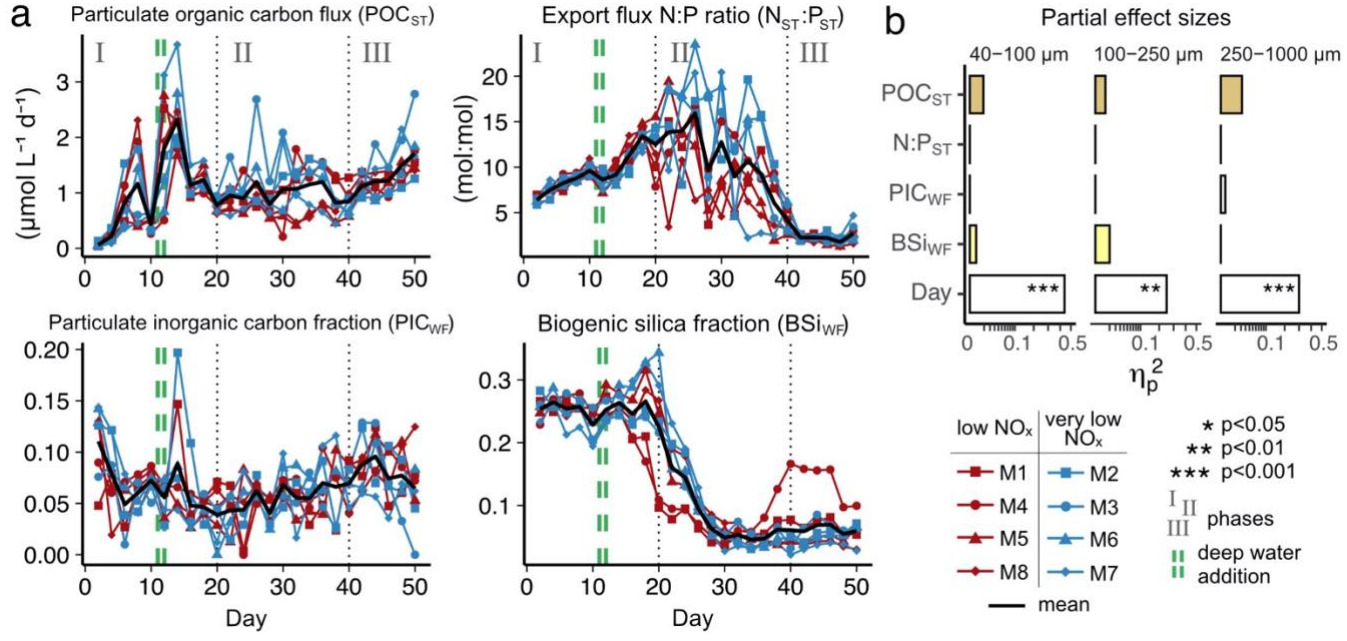

Figure 2. (**a**) Temporal development of key export parameters including absolute flux, elemental stoichiometry and mineral ballast (POC_{ST} and N_{ST}:P_{ST} modified from Bach et al. 2020). (**b**) Modelled effects of these parameters on particle sinking velocity (η_p^2: partial effect size).

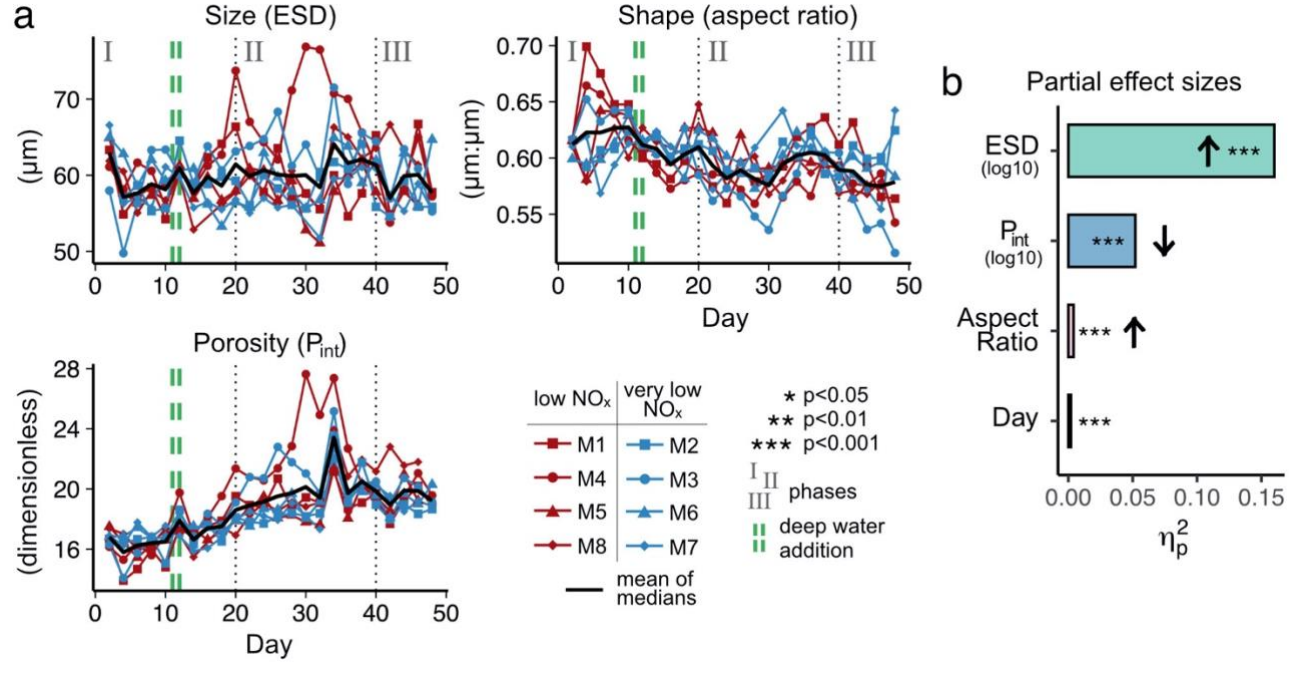

https://doi.org/10.5194/egusphere-2022-814
Preprint. Discussion started: 23 August 2022

Figure 3. (**a**) Temporal development of physical particle properties and (**b**) their effect on particle sinking velocity with effect directions indicated by arrows (up = positive, down = negative). The full statistical result, including interactions between the properties and day, are given in Table A3. Note that (**a**) shows daily median particle properties.

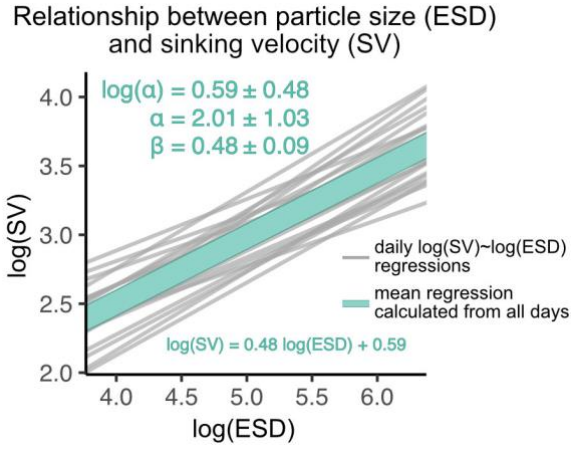

Figure 4. Size-sinking relationship of particles sampled from the sediment trap. Shown are the scaling factors α and β ± SD, as well as the mean regression model formula according to Eq. 3. This relationship was calculated in the 40–630 µm size range (see Sect. 2.3.1).